


Research Article

A Two-Phase Flow Model for Pressure Transient Analysis of Water Injection Well considering Water Imbibition in Natural Fractured Reservoirs

Mengmeng Li ¹, Qi Li,^{1,2} Gang Bi,² and Jiaen Lin²

¹College of Petroleum Engineering, China University of Petroleum Beijing, 102249 Beijing, China

²College of Petroleum Engineering, Xi'an Shiyou University, 710065 Xi'an, China

Correspondence should be addressed to Mengmeng Li; 2015312041@student.cup.edu.cn

Received 14 May 2018; Revised 30 July 2018; Accepted 19 August 2018; Published 4 September 2018

Academic Editor: Gilberto Espinosa-Paredes

Copyright © 2018 Mengmeng Li et al. This is an open access article distributed under the Creative Commons Attribution License, which permits unrestricted use, distribution, and reproduction in any medium, provided the original work is properly cited.

The pressure injection falloff test for water injection well has the advantages of briefness and convenience, with no effect on the oil production. It has been widely used in the oil field. Tremendous attention has been focused on oil-water two-phase flow model based on the Perrine-Martin theory. However, the saturation gradient is not considered in the Perrine-Martin method, which may result in errors in computation. Moreover, water imbibition is important for water flooding in natural fractured reservoirs, while the pressure transient analysis model has rarely considered water imbibition. In this paper, we proposed a semianalytical oil-water two-phase flow imbibition model for pressure transient analysis of a water injection well in natural fractured reservoirs. The parameters in this model, including total compressibility coefficient, interporosity flow coefficient, and total mobility, change with water saturation. The model was solved by Laplace transform finite-difference (LTFD) method coupled with the quasi-stationary method. Based on the solution, the model was verified by the analytical method and a field water injection test. The features of typical curves and the influences of the parameters on the typical curves were analyzed. Results show that the shape of pressure curves for single phase flow resembles two-phase flow, but the position of the two-phase flow curves is on the upper right of the single phase flow curves. The skin factor and wellbore storage coefficient mainly influence the peak value of the pressure derivatives and the straight line of the early period. The shape factor has a major effect on the position of the “dip” of pressure derivatives. The imbibition rate coefficient mainly influences the whole system radial flow period of the curves. This work provides valuable information in the design and evaluation of stimulation treatments in natural fractured reservoirs.

1. Introduction

The methods for pressure transient analysis of water injection well mostly still use the conventional well test method of single phase flow. Perrine [1] proposed to apply the single phase theory into the two-phase or multiphase well test theory by substitution of the single phase compressibility and mobility into the sum of total mobility and total compressibility of the multiphase system. Martin [2] provided the theoretical validation to Perrine's theory and indicated that the saturation gradient was neglected for Perrine's method. The total mobility, skin factor, and average formation pressure can be obtained based on this method. If it is a two-phase flow well test model of a water injection well, a multizone composite reservoir model [3–8] is used due to the different

properties of the injected fluid and the reservoir fluid. Within each region, the properties of the reservoir and fluid are constant, but it may be different for the two or three regions in a composite reservoir. The two or three zones for a composite reservoir were divided according to the formation and fluid properties. Some scholars [9–13] developed a two- or three-zone composite reservoir well test model by finite-difference or Laplace transformation method to get the pressure curves for water injection and pressure falloff period. However, these models assumed no saturation gradients within oil and water transition zone and the zone boundaries were virtually stationary before the well shut-in.

Actually, there were saturation discontinuities between the two or three fluid banks in a composite reservoir. A saturation gradient was formed after the water injection due

to the differences in oil and water properties. Weinstein [14] investigated the pressure-falloff data with a numerical model and suggested that the location of the fluid banks could be determined based on the Buckley-Leverett [15] frontal-advance equations. Sosa et al. examined the influence of saturation gradients on water injection pressure-falloff tests according to a two-phase radial numerical simulator [16]. It was further demonstrated that the radius of the fluid banks that was flooded completely by water should be estimated from the Buckley-Leverett theory rather than the technique mentioned in the previous literatures [17–19].

According to the Buckley-Leverett theory, the location of the front was estimated at any time during the injection period. The fluid bank can be discretized into a series of banks, so the water saturation distribution and the gradual change in fluid properties due to saturation gradients in the reservoir were obtained [20–24]. Chen [25] derived an approximate analytical solution for the pressure response during water injection/falloff test based on the front tracking method and Buckley-Leverett theory. Boughrara [26] added a two-phase term, which represents the existence of the two-phase zone and the movement of the water front, to the analytical single phase well test solution based on Buckley-Leverett equations for vertical and horizontal water injection wells. Zheng [27] developed a modified P-M approach for numerical well testing analysis of oil and water two-phase flowing reservoir on account of Buckley-Leverett equations. The water saturation distribution for a water injection well at any time can be obtained with the Buckley-Leverett frontal-advance equations [28–30].

Based on the quasi-stationary method [31–33], the saturation was decoupled from the pressure with the Buckley-Leverett theory. Therefore, the water saturation can be considered as constants when the diffusivity equation was solved simultaneously for water injection well test analysis. On the basis of the Buckley-Leverett equations, De Swaan calculated the rate of water imbibition in a fracture surrounded by matrix in a convolution form [34, 35]. Kazemi [36] proposed an analytical solution for Buckley-Leverett equations in a fracture surrounded by matrix undergoing imbibition. By extending the linear Buckley-Leverett formula considering imbibition to a radial flow system for the naturally fractured reservoir [37], the water saturation can be estimated according to the radial flow model.

In this work, an oil-water two-phase flow imbibition well test model of a water injection well in natural fractured reservoirs was developed and solved by the LTFD method coupled with the quasi-stationary method. The LTFD method transformed the equations into Laplace domain and eliminated the need for time discretization; thus, the method was semianalytical in time and the stability and convergence problems in temporal domain were avoided [38, 39]. According to analysis of the pressure falloff data, the features of the typical curves of oil-water two-phase flow considering water imbibition were analyzed. The effect of the imbibition rate coefficient, skin factor, wellbore storage coefficient, shape factor, and boundary conditions on the typical curves was also investigated. New ideas had been put forward in accordance with the analysis above.

2. Model Description

In order to calculate the saturation and pressure of the diffusivity equation in the two-phase pressure transient model simultaneously, the quasi-stationary method was adopted by decoupling the saturation from the pressure on account of the Buckley-Leverett water displacement theory.

2.1. Water Saturation Model. The water saturation distribution in the fracture and matrix considering water imbibition was estimated by integrating empirical matrix fracture transfer functions into the Buckley-Leverett equation. Based on the assumption that the cumulative oil recovery from a piece of rock surrounded by water is a continuous monotonic function of time and converges to a finite limit, Arnofsky et al. [34] proposed an exponential equation for oil recovery estimation of water displacement considering water imbibition in a fractured reservoir as shown:

$$R = R_{\infty} (1 - e^{-Rt}) \quad (1)$$

where

$$R_{\infty} = \emptyset_m (1 - s_{orm} - s_{wcm}) \quad (2)$$

$$R = \emptyset_m (s_m - s_{wcm}) \quad (3)$$

Considering the gradual variation of the water saturation in surrounding fractures, De Swaan [35] calculated the rate of water imbibition in a fracture surrounded by matrix in a convolution form. Kazemi [36] proposed an analytical solution for a linear flow system that accounts for saturation changes in fracture and matrix. Shimamoto [37] extended the formula to a radial flow system for the Warrant-Root model with the volume conservation in a fracture.

The water saturation change in the fracture can be expressed as

$$-\frac{q}{2\pi rh} \frac{\partial s_{wf}}{\partial r} - R_c R_{\infty} \int_0^t e^{-R_c(t-\tau)} \frac{\partial s_{wf}}{\partial \tau} d\tau = \emptyset_f \frac{\partial s_{wf}}{\partial t} \quad (4)$$

And the water saturation in the matrix can be written as

$$R_c R_{\infty} \int_0^t e^{-R_c(t-\tau)} \frac{\partial s_{wf}}{\partial \tau} d\tau = \emptyset_m \frac{\partial s_{wm}}{\partial t} \quad (5)$$

The initial and boundary condition

$$s_{wf}(r=0, t) = 1 \quad (6)$$

$$s_{wf}(r, t=0) = 0 \quad (7)$$

Introducing Laplace transform, the water saturation in Laplace domain can be expressed as

$$\bar{s}_{wf} = \frac{1}{z_1} e^{-(z_1\beta/(R_c+z_1)+z_1\alpha)} \quad (8)$$

$$\bar{s}_{wm} = \frac{s_{wm}(r, t=0)}{z_1} + \frac{R_c R_{\infty}}{\emptyset_m} \frac{e^{-(z_1\beta/(R_c+z_1)+z_1\alpha)}}{z_1 (R_c + z_1)} \quad (9)$$

where z_1 is Laplace variable,

$$\alpha = \frac{\pi h r^2}{q} \emptyset_f \quad (10)$$

$$\beta = \frac{\pi h r^2}{q} R_c R_{\infty} \quad (11)$$

The water saturation in fracture and matrix in the real domain can be obtained by inversion of Laplace transform

$$s_{wf}(r, t) = \begin{cases} 0 & (t < \alpha) \\ e^{-\beta} \left[e^{-R_c(t-\alpha)} I_0 \left(2\sqrt{\beta R_c(t-\alpha)} \right) + R_c \int_{\alpha}^t e^{-R_c(\tau-\alpha)} I_0 \left(2\sqrt{\beta R_c(\tau-\alpha)} \right) d\tau \right] & (t \geq \alpha) \end{cases} \quad (12)$$

$$s_{wm}(r, t) = \begin{cases} s_{wcm} & (t < \alpha) \\ s_{wcm} + (1 - s_{orm} - s_{wcm}) R_c e^{-\beta} \int_{\alpha}^t e^{-R_c(\tau-\alpha)} I_0 \left(2\sqrt{\beta R_c(\tau-\alpha)} \right) d\tau & (t \geq \alpha) \end{cases} \quad (13)$$

2.2. Pressure Transient Model

2.2.1. Physical Model. The naturally fractured reservoir is described by the Warren-Root model with constant temperature and uniform initial pressure. The reservoir is assumed to be a homogeneous horizontal radial reservoir with an upper and lower sealed boundary. The slightly compressible fluids (water and oil) flowing in the matrix and fracture system obey Darcy's law, and the mass exchange between matrix and fracture system is assumed to be pseudosteady [40]. The gravity effect of the 2D system is neglected. A fully penetrating water injection well with constant injection rate is located in the center of the reservoir. As the water injection into the formation, the water saturation changes with time and space. A moving interface divided the radial formation into two regions, as shown in Figure 1. From the figure, r_f indicates the position of water drive front. Region 1 is the water invaded region and region 2 is the uninvaded region.

2.2.2. Mathematical Model. After the water saturation distribution at any time during the injection period was obtained, the pressure equations can be solved by the quasi-stationary and LTFD method. According to the double porosity model proposed by Warren and Root, an oil-water two-phase flow well test model considering the saturation gradients within each region with a moving boundary between the regions for a water injection well was proposed as follows:

Fracture system

$$\frac{1}{r} \frac{\partial}{\partial r} \left(r \frac{k_f k_{rof}}{\mu_o B_o} \frac{\partial p_f}{\partial r} \right) - \tau_{omf} = \frac{\partial}{\partial t} \left(\frac{\emptyset_f S_{of}}{B_o} \right) \quad (14)$$

$$\frac{1}{r} \frac{\partial}{\partial r} \left(r \frac{k_f k_{rwf}}{\mu_w B_w} \frac{\partial p_f}{\partial r} \right) - \tau_{wmf} = \frac{\partial}{\partial t} \left(\frac{\emptyset_f S_{wf}}{B_w} \right) \quad (15)$$

Matrix system

$$\tau_{omf} = \frac{\partial}{\partial t} \left(\frac{\emptyset_m S_{om}}{B_o} \right) \quad (16)$$

$$\tau_{wmf} = \frac{\partial}{\partial t} \left(\frac{\emptyset_m S_{wm}}{B_w} \right) \quad (17)$$

Matrix and fracture transfer equations

$$\tau_{omf} = \frac{F_s k_m k_{rom}}{\mu_o B_o} (p_f - p_m) \quad (18)$$

$$\tau_{wmf} = \frac{F_s k_m k_{rwm}}{\mu_w B_w} (p_f - p_m) \quad (19)$$

Substituting (16) and (17) into (14) and (15) and (18) and (19) yields

$$\frac{1}{r} \frac{\partial}{\partial r} \left(r M_{tf} \frac{\partial p_f}{\partial r} \right) = \emptyset_f C_{tf} \frac{\partial p_f}{\partial t} + \emptyset_m C_{tm} \frac{\partial p_m}{\partial t} \quad (20)$$

$$\emptyset_m C_{tm} \frac{\partial p_m}{\partial t} = F_s M_{tu} (p_f - p_m) \quad (21)$$

where M_{tf} denotes the total mobility of fracture system and M_{tu} is the mobility between fracture and matrix. The subscript "u" represents "upstream saturation". For water injection period, the water flows from fracture to matrix, so water saturation in the fracture is used for the relative permeability evaluation (see (23)). Inversely, water saturation

in the matrix is applied to calculate the relative permeability during the falloff period (see (24)).

$$M_{tf} = k_f \left(\frac{k_{rof}(S_{wf})}{\mu_o} + \frac{k_{rwf}(S_{wf})}{\mu_w} \right) \quad (22)$$

$$M_{tu} = k_m \left(\frac{k_{rom}(S_{wf})}{\mu_o} + \frac{k_{rwm}(S_{wf})}{\mu_w} \right) \quad (23)$$

$$M_{tu} = k_m \left(\frac{k_{rom}(S_{wm})}{\mu_o} + \frac{k_{rwm}(S_{wm})}{\mu_w} \right) \quad (24)$$

In order to simplify the calculation, a set of dimensionless variables were introduced as listed in Table 1. Equations (20) and (21) and the initial and boundary conditions can be written in dimensionless form

$$\frac{1}{r_D} \frac{\partial}{\partial r_D} \left(r_D M_{tfD} \frac{\partial p_{fD}}{\partial r_D} \right) = \omega_1 \frac{\partial p_{fD}}{\partial t_D} + \omega_2 \frac{\partial p_{mD}}{\partial t_D} \quad (25)$$

$$\omega_2 \frac{\partial p_{mD}}{\partial t_D} = \lambda (p_{fD} - p_{mD}) \quad (26)$$

The initial condition

$$p_{fD}(r_D, t_D = 0) = 0 \quad (27)$$

$$p_{mD}(r_D, t_D = 0) = 0 \quad (28)$$

The inner boundary condition considering the skin effect is

$$p_{wD} = \left(p_{fD} - S r_D \frac{\partial p_{fD}}{\partial r_D} \right)_{r_D=1} \quad (29)$$

The inner boundary condition considering wellbore storage effect is

$$C_D \frac{dp_{wD}}{dt_D} - \left(r_D \frac{\partial p_{fD}}{\partial r_D} \right)_{r_D=1} = 1 \quad (30)$$

The constant pressure outer boundary condition is

$$p_{fD}(r_D = r_{eD}, t_D) = 0 \quad (31)$$

$$p_{mD}(r_D = r_{eD}, t_D) = 0 \quad (32)$$

The no flow outer boundary condition is

$$\left(\frac{\partial p_{fD}}{\partial r_D} \right)_{r_D=r_{eD}} = 0 \quad (33)$$

$$\left(\frac{\partial p_{mD}}{\partial r_D} \right)_{r_D=r_{eD}} = 0 \quad (34)$$

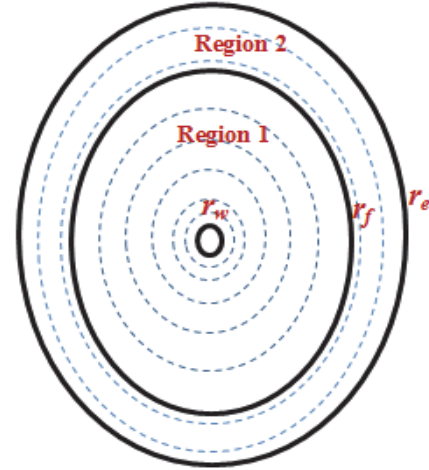


FIGURE 1: Schematic of two-zone composite reservoir.

To simplify the computation, a logarithmic transform, $z = \ln(r_D)$, and the Laplace transform with the quasi-stationary assumption were used. Thus, (25)–(34) can be rewritten as

$$\frac{1}{e^{2z}} \frac{d}{dz} \left(M_{tfD} \frac{d\bar{p}_{fD}}{dz} \right) = \omega_1 [u\bar{p}_{fD} - p_{fD}(z, 0)] \quad (35)$$

$$+ \omega_2 [u\bar{p}_{mD} - p_{mD}(z, 0)]$$

$$\omega_2 [u\bar{p}_{mD} - p_{mD}(z, 0)] = \lambda (\bar{p}_{fD} - \bar{p}_{mD}) \quad (36)$$

The initial condition is

$$p_{fD}(t_D = 0) = 0 \quad (37)$$

$$p_{mD}(t_D = 0) = 0 \quad (38)$$

The inner boundary condition considering the skin effect is

$$\bar{p}_{wD} = \left(\bar{p}_{fD} - S \frac{d\bar{p}_{fD}}{dz} \right)_{z=0} \quad (39)$$

The inner boundary condition considering wellbore storage effect is

$$\left(\frac{d\bar{p}_{fD}}{dz} \right)_{z=0} - C_D [u\bar{p}_{wD} - p_{wD}(t_D = 0)] = -\frac{1}{u} \quad (40)$$

The constant pressure outer boundary condition is

$$\bar{p}_{fD}(z = z_e) = 0 \quad (41)$$

$$\bar{p}_{mD}(z = z_e) = 0 \quad (42)$$

TABLE I: Dimensionless variable for pressure calculation.

$\widehat{M}_{tf} = k_f \left(\frac{k_{rof}(S_{wf} = 1)}{\mu_o} + \frac{k_{rwf}(S_{wf} = 1)}{\mu_w} \right)$	$M_{tfD} = \frac{M_{tf}}{\widehat{M}_{tf}}$
$P_{fD} = \frac{2\pi\widehat{M}_{tf}h}{qB_w} (p_f - p_i)$	$\lambda = \frac{F_S r_w^2 M_{tu}}{\widehat{M}_{tf}}$
$P_{mD} = \frac{2\pi\widehat{M}_{tf}h}{qB_w} (p_m - p_i)$	$r_D = \frac{r}{r_w}$
$\widehat{C}_{tf} = C_r + C_w S_{wi} + C_o (1 - S_{wi})$	$\omega_1 = \frac{r}{\theta_f \widehat{C}_{tf}}$
$\widehat{C}_{tm} = C_r + C_w S_{wcm} + C_o (1 - S_{wcm})$	$\omega_2 = \frac{\theta_m \widehat{C}_{tm}}{(\theta_f \widehat{C}_{tf} + \theta_m \widehat{C}_{tm})}$
$t_D = \frac{\widehat{M}_{tf}}{(\theta_f \widehat{C}_{tf} + \theta_m \widehat{C}_{tm}) r_w^2}$	$C_D = \frac{C}{2\pi(\theta_f \widehat{C}_{tf} + \theta_m \widehat{C}_{tm}) h r_w^2}$

The no flow outer boundary condition is

$$\left(\frac{d\bar{p}_{fD}}{dz} \right)_{z=z_e} = 0 \quad (43)$$

$$\left(\frac{d\bar{p}_{mD}}{dz} \right)_{z=z_e} = 0 \quad (44)$$

The pressure change near the wellbore was relatively larger than the area away from the bottom of the well. So the formation was divided into n grid blocks in radial direction according to the point-centered logarithmic gridding method, which was shown as the dotted blue line in Figure 1. By using finite-difference approximation, (35)–(44) can be written as

$$a_i \bar{p}_{fDi} + b_i \bar{p}_{fDi+1} + c_i \bar{p}_{fDi+2} = d_i \quad (45)$$

$$\bar{p}_{mDi} = \frac{\lambda \bar{p}_{fDi} + \omega_2 p_{mD}(t_D = 0)}{\omega_2 u + \lambda} \quad (46)$$

where

$$a_i = \mu_w \left(\frac{k_{rof}(S_{wf}(r_{i-1}, t))}{\mu_o} + \frac{k_{rwf}(S_{wf}(r_{i-1}, t))}{\mu_w} \right) \quad (47)$$

$$b_i = - \left[a_i + c_i + \left(\frac{\omega_1 \omega_2 u^2 + \omega_1 \lambda u + \omega_2 \lambda u}{\omega_2 u + \lambda} \right)_i e^{2i\Delta z} \Delta z^2 \right] \quad (48)$$

$$c_i = \mu_w \left(\frac{k_{rof}(S_{wf}(r_i, t))}{\mu_o} + \frac{k_{rwf}(S_{wf}(r_i, t))}{\mu_w} \right) \quad (49)$$

$$d_i = - \left[e^{2i\Delta z} \Delta z^2 \omega_{1i} P_{fDi}(t_D = 0) + e^{2i\Delta z} \Delta z^2 \left(\frac{\omega_2 \lambda}{\omega_2 u + \lambda} \right)_i P_{mDi}(t_D = 0) \right] \quad (50)$$

The inner boundary condition is

$$e_1 \bar{p}_{wD} + e_2 \bar{p}_{fD0} + e_3 \bar{p}_{fD1} = e_8 \quad (51)$$

$$e_4 \bar{p}_{fD0} + e_5 \bar{p}_{fD1} = e_9 \quad (52)$$

The outer boundary condition is

$$e_6 \bar{p}_{fDn-1} - e_7 \bar{p}_{fDn} = 0 \quad (53)$$

The coefficients for different boundary conditions are shown in Table 2.

The pressure difference equations ((45) and (46)) can be written in a matrix form as

$$M \vec{x} = \vec{b} \quad (54)$$

where M is a large sparse matrix, \vec{x} is the unknown pressure vector, and \vec{b} is the known vector related to the initial and

TABLE 2: Coefficients with different boundary conditions.

Boundary conditions	Coefficients
Constant pressure outer boundary	$e_1 = 1, e_2 = -(1 + \frac{S}{\Delta z}), e_3 = \frac{S}{\Delta z},$ $e_4 = 1 + \Delta z C_D u + S C_D u, e_5 = -S C_D u - 1, e_6 = 0$ $e_7 = 1, e_8 = 0, e_9 = \frac{\Delta z}{u} - \Delta z C_D p_{wD}(t_D = 0)$
No flow outer boundary	$e_1 = 1, e_2 = -(1 + \frac{S}{\Delta z}), e_3 = \frac{S}{\Delta z}, e_4 = 1 + \Delta z C_D u + S C_D u$ $e_5 = -S C_D u - 1, e_6 = a_{n-1} + c_{n-1}$ $e_7 = b_{n-1}, e_8 = 0, e_9 = \frac{\Delta z}{u} - \Delta z C_D p_{wD}(t_D = 0)$

boundary conditions. The matrix M and vectors \vec{x} and \vec{b} can be explicitly given as

$$M = \begin{bmatrix} e_1 & e_2 & e_3 & 0 & 0 & 0 & 0 & 0 & 0 \\ 0 & e_4 & e_5 & 0 & 0 & 0 & 0 & 0 & 0 \\ 0 & 0 & a_1 & b_1 & c_1 & 0 & \dots & 0 & 0 & 0 \\ 0 & 0 & 0 & a_2 & b_2 & c_2 & & 0 & 0 & 0 \\ \vdots & & & & & & & & & \\ 0 & 0 & 0 & 0 & 0 & 0 & & a_{n-3} & b_{n-3} & c_{n-3} \\ 0 & 0 & 0 & 0 & 0 & 0 & \dots & a_{n-2} & b_{n-2} & c_{n-2} \\ 0 & 0 & 0 & 0 & 0 & 0 & & 0 & e_6 & e_7 \end{bmatrix} \quad (55)$$

$$\vec{x} = \begin{bmatrix} \bar{p}_{wD} \\ \bar{p}_{fD_0} \\ \bar{p}_{fD_1} \\ \bar{p}_{fD_2} \\ \vdots \\ \vdots \\ \bar{p}_{fD_{n-1}} \end{bmatrix} \quad (56)$$

$$\vec{b} = \begin{bmatrix} e_8 \\ e_9 \\ d_1 \\ d_2 \\ \vdots \\ \vdots \\ d_{n-1} \end{bmatrix} \quad (57)$$

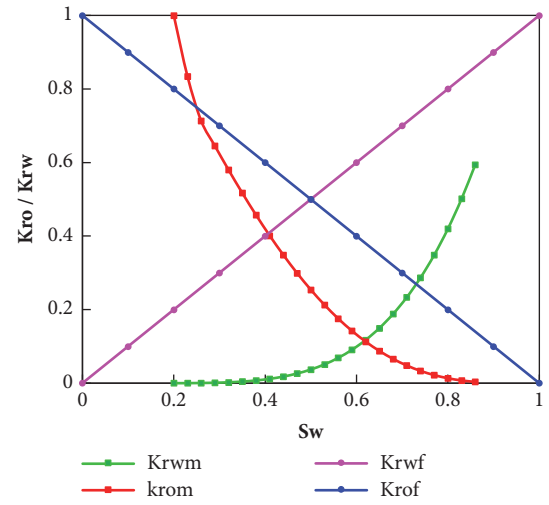


FIGURE 2: Curves of relative permeability of oil and water in fracture and matrix.

The unknown vector \vec{x} was calculated by using the Stehfest algorithm. Therefore, the dimensionless pressure and pressure derivatives [41] at the bottom of the wellbore can be plotted according to the solutions of the formulated mathematical model for the water injection system. The basic parameters and the relative permeability data for the calculation of pressure curves are illustrated in Table 3 and Figure 2.

3. Verification of the Mathematical Model

Because little was available in the literatures for pressure behavior of a water injection well considering saturation gradient and water imbibition in dual-porosity reservoir by LTFD method, the model solutions were validated by simplifying the model into a single phase water injection well in a dual-porosity system, which was compared to the conventional analytical solution [42] by commercial software as shown in Figure 3. From the figure, the LTFD results show good agreement with the analytical solution.

Moreover, a field water injection test was used to further verify the proposed model. The basic information of the water injection well and the relative permeability data was listed in Table 4 and Figure 4. And Figure 5 shows the pressure curves

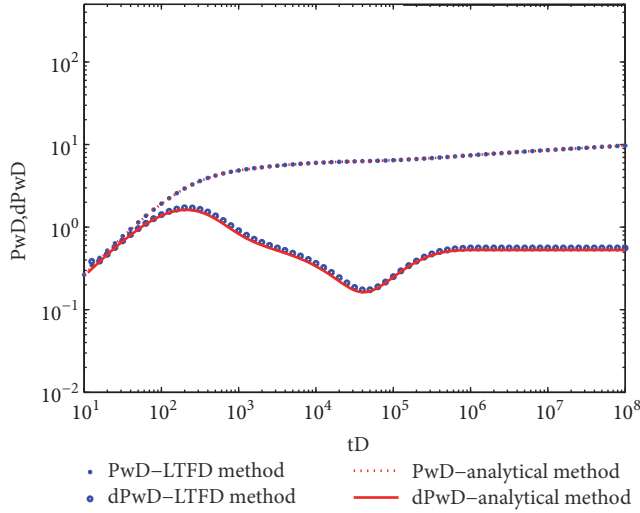


FIGURE 3: Comparison of the results by LTFD method and analytical method.

TABLE 3: Basic parameters for calculation of pressure curves.

Parameter	Value	Units
Formation height	10	m
Fracture porosity	0.03	fraction
Matrix porosity	0.27	fraction
Wellbore radius	0.1	m
Fracture permeability	0.6	μm^2
Matrix permeability	6×10^{-5}	μm^2
Irreducible water saturation	20	%
Residual oil saturation	14	%
Oil volume factor	1.03	fraction
Water volume factor	1	fraction
Shape factor	6×10^{-4}	$1/\text{cm}^2$
Oil viscosity	1	mPa.s
Water viscosity	0.5	mPa.s
rock compressibility	6×10^{-4}	1/MPa
oil compressibility	1×10^{-3}	1/MPa
water compressibility	4×10^{-4}	1/MPa
Injection rate	30	m^3/day
Initial pressure	14	MPa
Skin factor	0.1	fraction
Imbibition rate coefficient	0.1	1/day
Wellbore storage coefficient	0.01	lm^3/MPa

of the well test data comparing with the results in our model. From the figure, it is found that our results match well with the field test data.

4. Model Features Analysis

The pressure curves of oil-water two-phase flow considering water imbibition and the saturation gradients during injection period by the LTFD method were plotted in this section. The behaviors of the typical curves were analyzed by

TABLE 4: Basic information of the water injection well.

Parameter	Value	Units
Formation height	12.6	m
Fracture porosity	0.03	fraction
Matrix porosity	0.268	fraction
Wellbore radius	0.12	m
Oil volume factor	1.163	fraction
Water volume factor	1	fraction
Oil viscosity	9.6	mPa.s
Water viscosity	0.5	mPa.s
rock compressibility	5×10^{-4}	1/MPa
oil compressibility	4.8×10^{-3}	1/MPa
water compressibility	3.9×10^{-4}	1/MPa
Injection rate	256	m^3/day
Initial pressure	15	MPa

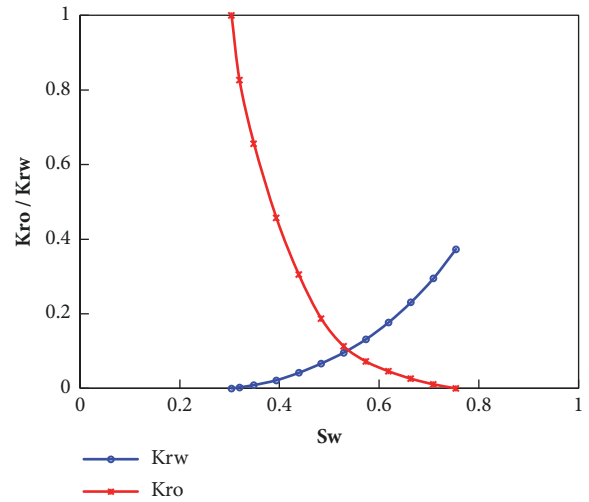


FIGURE 4: The relative permeability of oil and water for the water injection well.

comparing the typical curves of single phase flow with the two-phase flow curves in the fractured reservoirs as follows.

4.1. Features of Typical Curves. Figure 6 illustrates the pressure curves of single phase flow and oil-water two-phase flow in fractured reservoirs by LTFD method without water imbibition. According to the feature of the curves, the formation flow can be divided into three stages. The first stage is the flow in the fracture system, the second stage is the flow between the fracture and the matrix system, and the third stage is the flow in the whole system, including the fracture and matrix. The figure shows that the shape of curves for single phase flow and two-phase flow is similar, but the position of the two-phase flow curves is on the upper right of the single phase flow curves. The reason is that when oil and water exist in the whole system, the total mobility of oil and water is lower than the single phase, and the bottom-hole pressure increases more quickly as the fluid is injected

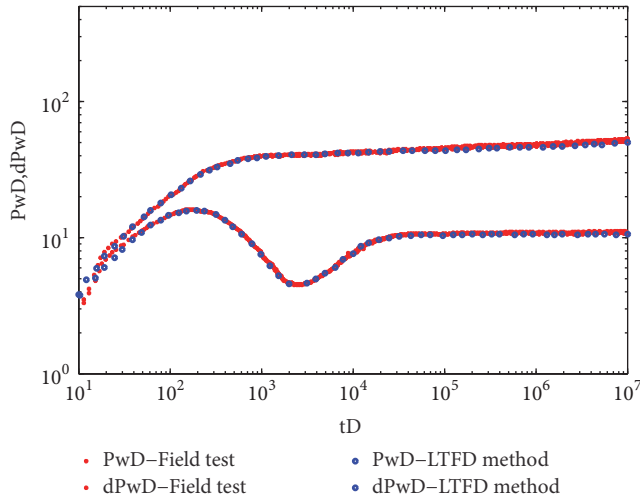


FIGURE 5: Comparison of the results in this work and the field injection test.

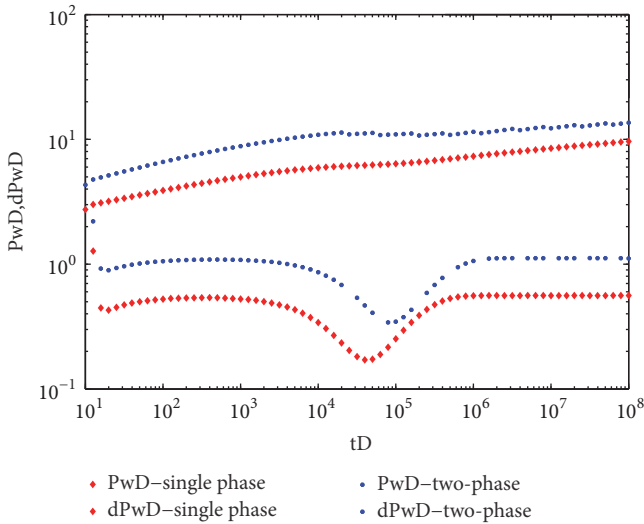


FIGURE 6: Typical curves of single phase and two-phase flow during injection period.

into the well. Thus, the pressure derivative curves of two-phase flow move upward compared to the single phase flow curves. Moreover, due to the decrease of the total mobility, the interporosity flow capacity between matrix and fracture system decreases when the single phase flow becomes two-phase flow. Thus, the “dip” of the two-phase flow curves occurs later than that of the single phase flow curves.

4.2. Effects of Parameters. The key factors influencing the pressure behavior of water injection period including skin factor, wellbore storage coefficient, shape factor, water imbibition rate coefficient, and boundary conditions were discussed in detail in this part.

4.2.1. Skin Factor. Figure 7 shows the effect of skin factor on the pressure curves of the water injection well. The solid

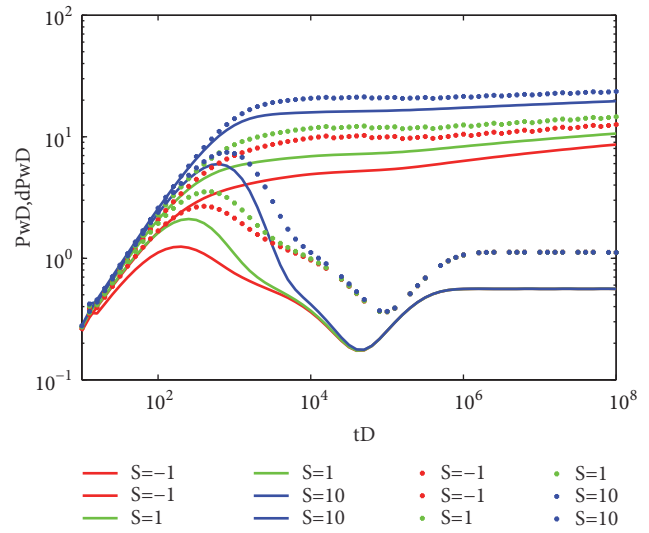


FIGURE 7: Influence of different skin factors on pressure transient behavior.

lines are the curves of single phase flow and the circles are oil-water two-phase flow curves. The red, green, and blue colors indicate that the shape factor values are -1, 1, and 10, respectively. From the figure, the skin factor mainly influences the peak value of the pressure derivatives. As the value of skin factor increases, the peak value gets higher and the time for peak value occurrence becomes later which indicates that the reservoir is more severely contaminated. The pressure derivative curves of two-phase flow move toward the upper right of the single phase flow curves, which shows the same change rule with Figure 6. When the skin factor becomes larger, the peak value difference between the single phase and two-phase decreases, and the inclination of the curves after the peak value increases.

4.2.2. Wellbore Storage Coefficient. Figure 8 is the influences of wellbore storage coefficient on the pressure and pressure derivative curves of the water injection well. The red, green, and blue colors indicate that wellbore storage coefficient values are 0.01, 0.1, and 1, respectively. As seen, the main difference of the curves occurs on the straight line of early period. As the wellbore storage coefficient increases, the straight line section becomes longer and the time of peak value occurs later. Besides, the wellbore storage effect will cover up the radial flow stage in the fracture system, directly going to the transitional flow stage between the fracture and matrix. The pressure derivative curves of two-phase flow move upper right to the single phase flow curves after the straight line of wellbore storage stage, which agrees with the change rule of Figure 6.

4.2.3. Shape Factor. The influences of shape factor on the pressure curves of the water injection well are shown in Figure 9. The red, green, and blue colors indicate that shape factor values are 10^{-5} , 10^{-4} , and 10^{-3} , respectively. By comparison of the curves, it is found that the shape

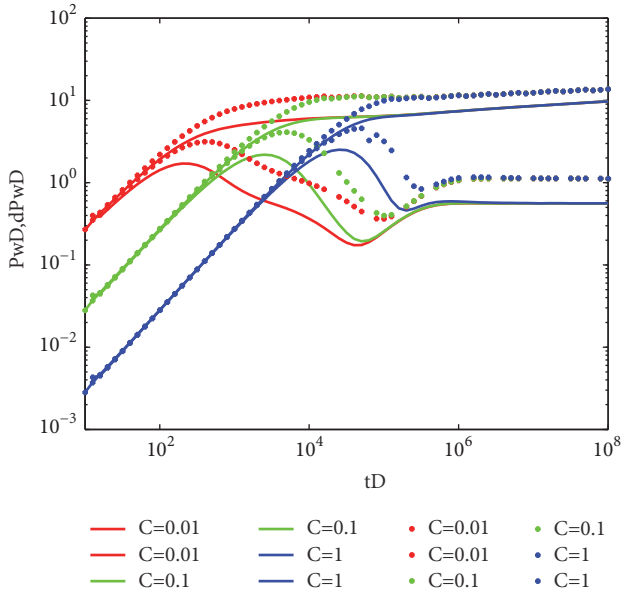


FIGURE 8: Influence of different wellbore storage coefficients on pressure transient behavior.

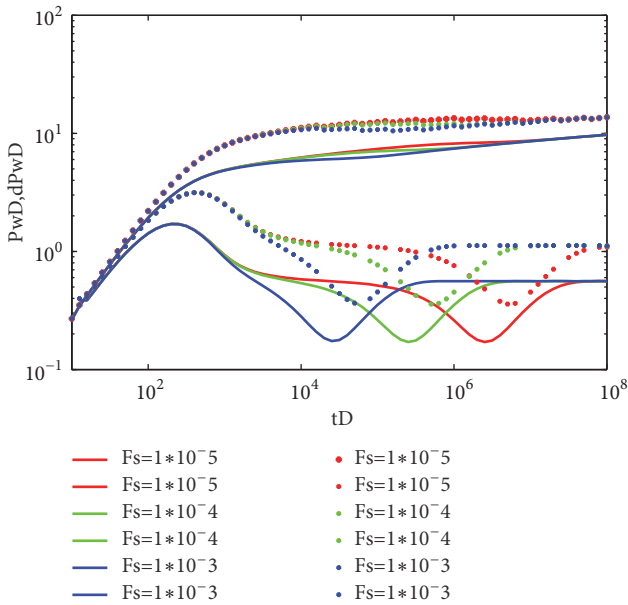


FIGURE 9: Influence of different shape factors on pressure transient behavior.

factor mainly has an effect on the position of the “dip” of the pressure derivatives. When the value of shape factor gets greater, the “dip” appears earlier and the “dip” moves closer to the left. The main reason is that the shape factor is a component of the equation defining the interporosity parameter. The higher the shape factor is, the easier the fluid exchange between the fracture and matrix is and the earlier the transitional flow stage occurs. It also demonstrates that the pressure derivative curves of two-phase flow move upper right to the single phase flow curves, which is in line with the change rule of Figure 6.

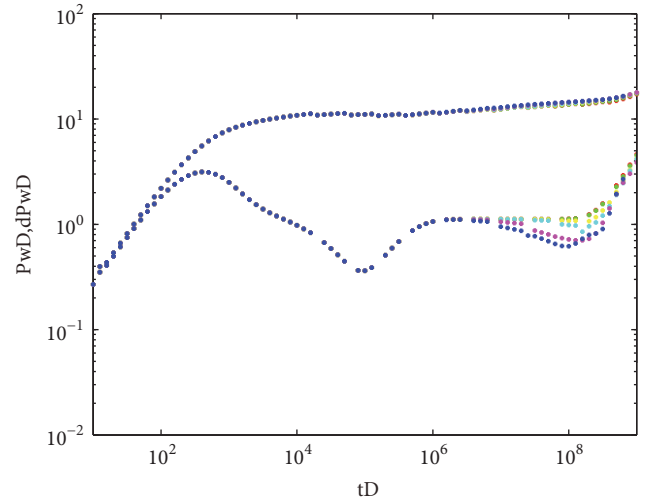


FIGURE 10: Pressure behavior of different imbibition rate coefficients with no flow outer boundary.

4.2.4. Imbibition Rate Coefficient with No Flow Outer Boundary Condition. Figure 10 describes the pressure behavior of the water injection well under no flow outer boundary condition when the water imbibition rate coefficient values are 0, 0.01, 0.05, 0.1, 0.5, and 1, respectively. From the figure, the imbibition rate coefficient mainly has an effect on the whole system (matrix and fracture system) radial flow period of the curves. As the imbibition rate coefficient becomes larger, there are more fluid exchange between the fracture and matrix, and more fluid supply from the matrix to the fracture. The water imbibition process is slow, so there is a second interporosity period after the whole system radial flow period. And with the increase of water imbibition rate coefficient, the pressure derivative curves dip downward earlier and the degree for the curves dropping down becomes larger. After that, the pressure derivative curves rise up to a uniform line with the same slope due to the influence of the no flow outer boundary.

4.2.5. Imbibition Rate Coefficient with Constant Pressure Boundary Condition. Figure 11 shows the pressure and pressure derivative curves of the water injection well under constant pressure boundary condition when the water imbibition rate coefficient values are 0, 0.01, 0.05, 0.1, 0.5, and 1, respectively. By comparison and analysis, it is concluded that the pressure derivative curve is a straight line at the whole system radial flow period when no water imbibition is considered. When considering water imbibition, the pressure derivatives decline at the whole system radial flow period. The pressure derivatives drop downward more and earlier with the increase of imbibition rate coefficient. After that, the curves also drop down due to the constant pressure outer boundary effect.

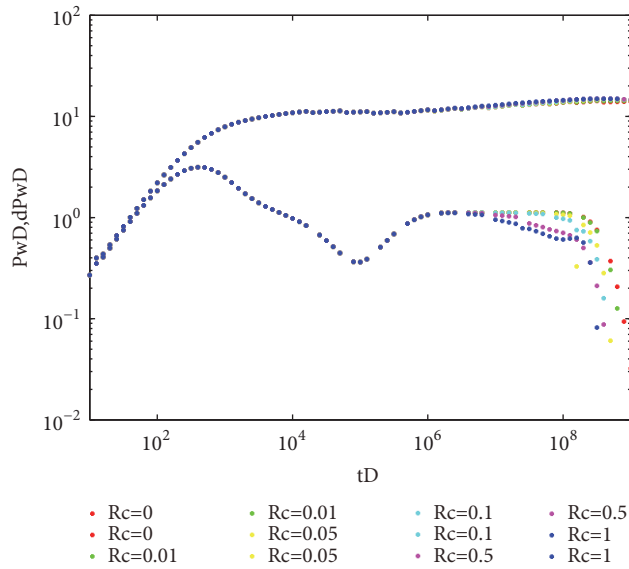


FIGURE 11: Pressure behavior of different imbibition rate coefficients with constant pressure boundary.

5. Conclusions

In this work, a semianalytical two-phase flow model considering water imbibition and the saturation gradients within each region during injection period was proposed to analyze the pressure transient behavior of the water injection well in fractured reservoirs. Validation of the presented model was performed by analytical method and a field water injection test. The model features were investigated by sensitivity analysis. Some conclusions were drawn as follows:

- (1) The shape of the pressure curves for the proposed model is similar to the single phase flow model, while the position of the curves for the two-phase flow model is on the upper right of the single phase flow model.
- (2) The main influence of skin factor on the curves occurs on the peak value of the pressure derivatives. As the skin factor becomes larger, the peak value difference between single phase and two-phase pressure curves decreases, and the inclination of the curves after the peak value increases.
- (3) The wellbore storage coefficient mainly has an effect on the straight line of the early period for the pressure curves. The shape factor mainly has an effect on the position of the “dip” of the pressure derivatives which is the same as the interporosity parameter.
- (4) The imbibition rate coefficient mainly influences the whole system radial flow period of the pressure curves. The pressure derivative curves dip downward earlier and drop down to a greater degree with the increase of imbibition rate coefficient.

Nomenclature

R:	Recovery, fraction
R_c :	Imbibition rate coefficient, 1/day
R_{∞} :	Ultimate cumulative oil recovery, fraction
\emptyset :	Porosity, fraction
s_{or} :	Residual oil saturation, fraction
s_{wc} :	Irreducible water saturation, fraction
s_w :	Water saturation, fraction
z :	Logarithmic transform variable, dimensionless
u :	Laplace variable, dimensionless
q :	Displacement rate, m^3/d
t :	Time, h
k :	Permeability, μm^2
k_r :	Relative permeability, fraction
h :	Formation height, m
r :	Radial distance, m
r_w :	Wellbore radius, m
p :	Pressure, MPa
μ :	Viscosity, mPa·s
B :	Formation volume factor, dimensionless
τ :	Fracture matrix transfer term, m^3/d
F_s :	Shape factor, $1/m^2$
C_t :	Total compressibility, 1/MPa
M_t :	Total mobility, 1/MPa
λ :	Interporosity flow coefficient, fraction
ω :	Storativity ratio, fraction
S :	Skin factor, dimensionless
C :	Wellbore storage coefficient, m^3/MPa

Subscripts

f:	Fracture
m:	Matrix
o:	Oil
w:	Water
t:	Total
e:	External
D:	Dimensionless variable

Superscripts

-:	Laplace-transformed variable
$\hat{}$:	Endpoint property
\rightarrow :	Vector symbol.

Data Availability

The data used to support the findings of this study are available from the corresponding author upon request.

Conflicts of Interest

The authors declare that they have no conflicts of interest.

Acknowledgments

The authors gratefully acknowledge the support of the National Basic Research 973 Program of China (Grant No.

2015CB250900), the National Natural Science Foundation of China (Grant No. 51704237), and the Research Projects of Shaanxi Provincial Education Department (Grant No. 13JS090).

References

- [1] R. L. Perrine, *Analysis of Pressure-buildup Curves*, vol. 56, American Petroleum Institute, 1956.
- [2] J. C. Martin, "Simplified Equations of Flow in Gas Drive Reservoirs and the Theoretical Foundation of Multiphase Pressure Buildup Analyses," *Society of Petroleum Engineers*, vol. 216, pp. 321–323, 1959.
- [3] W. Hurst, "Interference between Oil Field," *Transactions of the Metallurgical Society of AIME*, vol. 219, no. 8, pp. 175–192, 1960.
- [4] M. Mortada, "Oilfield Interference in Aquifers of Non-Uniform Properties," *Journal of Petroleum Technology*, vol. 12, no. 12, pp. 55–57, 2013.
- [5] T. Loucks and E. Guerrero, "Pressure Drop in a Composite Reservoir," *SPE Journal*, vol. 1, no. 03, pp. 170–176, 2013.
- [6] H. Bixel and H. Van Poolen, "Pressure Drawdown and Buildup in the Presence of Radial Discontinuities," *SPE Journal*, vol. 7, no. 03, pp. 301–309, 2013.
- [7] H. Ramey, "Approximate Solutions For Unsteady LiquidFlow In Composite Reservoirs," *Journal of Canadian Petroleum Technology*, vol. 9, no. 01, 2013.
- [8] Q. Deng, R. Nie, Y. Jia et al., "Pressure transient behavior of a fractured well in multi-region composite reservoirs," *Journal of Petroleum Science and Engineering*, vol. 158, pp. 535–553, 2017.
- [9] H. Kazemi, L. Merrill, and J. Jargon, "Problems in Interpretation of Pressure Fall-Off Tests in Reservoirs With And Without Fluid Banks," *Journal of Petroleum Technology*, vol. 24, no. 09, pp. 1147–1156, 2013.
- [10] L. Merrill, H. Kazemi, and W. B. Gogarty, "Pressure Falloff Analysis in Reservoirs With Fluid Banks," *Journal of Petroleum Technology*, vol. 26, no. 07, pp. 809–818, 2013.
- [11] A. Satman, M. Eggenschwiler, R. Tang, and R. H.J., "An analytical study of transient flow in systems with radial discontinuities," in *Proceedings of the SPE9399 presented at SPE Annual Technical Conference and Exhibition*, Dallas, Texas, TX, USA, September 1980.
- [12] A. Al-Bemani and I. Ershaghi, "Two-Phase Flow Interporosity Effects on Pressure Transient Test Response in Naturally Fractured Reservoirs," in *Proceedings of the SPE Annual Technical Conference and Exhibition*, Dallas, Texas.
- [13] Z. Chen, W. Yu, X. Liao, X. Zhao, Y. Chen, and K. Sepehrnoori, "A Two-Phase Flow Model for Fractured Horizontal Well with Complex Fracture Networks: Transient Analysis in Flowback Period," in *Proceedings of the SPE Liquids-Rich Basins Conference - North America*, Midland, Texas, USA.
- [14] H. G. Weinstein, "Cold Waterflooding a Warm Reservoir," in *Proceedings of the Fall Meeting of the Society of Petroleum Engineers of AIME*, Houston, Texas.
- [15] S. E. Buckley and M. C. Leverett, "Mechanism of fluid displacement in sands," *Transactions of the AIME*, vol. 146, no. 1, pp. 107–116, 2013.
- [16] A. Sosa, R. Raghavan, and T. Limon, "Effect of Relative Permeability and Mobility Ratio on Pressure Falloff Behavior," *Journal of Petroleum Technology*, vol. 33, no. 06, pp. 1125–1135, 2013.
- [17] P. Hazebroek, H. Rainbow, and CS. Matthews, "Pressure Fall-Off in Water Injection Wells," *Transactions of the Metallurgical Society of AIME*, vol. 213, pp. 250–260, 1958.
- [18] R. Carter, "Pressure Behavior of a Limited Circular Composite Reservoir," *SPE Journal*, vol. 6, no. 04, pp. 328–334, 2013.
- [19] A. Odeh, "Flow Test Analysis for a Well with Radial Discontinuity," *Journal of Petroleum Technology*, vol. 21, no. 02, pp. 207–210, 2013.
- [20] M. Abbaszadeh and M. Kamal, "Pressure-Transient Testing of Water-Injection Wells," *SPE Reservoir Engineering*, vol. 4, no. 01, pp. 115–124, 2013.
- [21] N. Yeh and R. Agarwal, "Pressure Transient Analysis of Injection Wells in Reservoirs With Multiple Fluid Banks," in *Proceedings of the SPE Annual Technical Conference and Exhibition*, San Antonio, Texas.
- [22] M. M. Levitan, "Application of water injection/falloff tests for reservoir appraisal: New analytical solution method for two-phase variable rate problems," *SPE Journal*, vol. 8, no. 4, pp. 341–349, 2003.
- [23] T. Nanba and R. Horne, "Estimation of Water and Oil Relative Permeabilities From Pressure Transient Analysis of Water Injection Well Data," in *Proceedings of the SPE Annual Technical Conference and Exhibition*, San Antonio, Texas.
- [24] R. B. Bratvold and R. N. Horne, "Analysis of pressure-falloff tests following cold-water injection," *SPE Formation Evaluation*, vol. 5, no. 3, pp. 293–302, 1990.
- [25] S. Chen, G. Li, and A. C. Reynolds, "Analytical Solution for Injection-Falloff-Production Test," in *Proceedings of the SPE Annual Technical Conference and Exhibition*, San Antonio, Texas, USA.
- [26] A. A. Boughrara, A. M. M. Peres, S. Chen, A. A. V. Machado, and A. C. Reynolds, "Approximate analytical solutions for the pressure response at a water-injection well," *SPE Journal*, vol. 12, no. 1, pp. 19–34, 2007.
- [27] S. Zheng and w. xu, "New approaches for analyzing transient pressure from oil and water two-phase flowing reservoir," in *Proceedings of the Kuwait International Petroleum Conference and Exhibition*, Kuwait City, Kuwait.
- [28] N. A. El-Khatib, "Transient Pressure Behavior of Composite Reservoirs with Moving Boundaries," in *Proceedings of the Middle East Oil Show and Conference*, Bahrain.
- [29] A. Dastan, M. M. Kamal, Y. Hwang, F. Suleen, and S. Morsy, "Falloff Testing Under Multiphase Flow Conditions in Naturally Fractured Reservoirs," in *Proceedings of the SPE Western Regional Meeting*, Garden Grove, California, USA.
- [30] C. n. Machado and A. C. Reynolds, "Approximate semi-analytical solution for injection-falloff-production well test: an analytical tool for the in situ estimation of relative permeability curves," *Transport in Porous Media*, vol. 121, no. 1, pp. 207–231, 2018.
- [31] T. Barkve, "Analytical study of reservoir pressure during water-injection well tests," *Society of Petroleum Engineers of AIME, (Paper) SPE*, 1986.
- [32] T. S. Ramakrishnan and F. J. Kuchuk, "Testing injection wells with rate and pressure data," *SPE Formation Evaluation*, vol. 9, no. 3, pp. 228–236, 1994.
- [33] L. G. Thompson and A. C. Reynolds, "Well testing for radially heterogeneous reservoirs under single and multiphase flow conditions," *SPE Formation Evaluation*, vol. 12, no. 1, pp. 57–64, 1997.

- [34] JS. Aronofsky, L. Masse, and SG. Natanson, "A Model for the Mechanism of Oil Recovery from the Porous Matrix Due to Water Invasion in Fractured Reservoirs," *Trans. AIME*, vol. 213, pp. 17–19, 1958.
- [35] A. de Swaan, "Theory of Waterflooding in Fractured Reservoirs," *SPE Journal*, vol. 18, no. 02, pp. 117–122, 2013.
- [36] H. Kazemi, J. Gilman, and A. Elsharkawy, "Analytical and Numerical Solution of Oil Recovery From Fractured Reservoirs With Empirical Transfer Functions (includes associated papers 25528 and 25818)," *SPE Reservoir Engineering*, vol. 7, no. 02, pp. 219–227, 2013.
- [37] T. Shimamoto, D. Kuramoto, N. Arihara, and T. Onishi, "A New Pressure Transient Analysis Model for Water Injection Well in Dual-Porosity Reservoirs," in *Proceedings of the SPE100881 presented at SPE Asia Pacific Oil & Gas Conference and Exhibition*, Adelaide, Australia, 2006.
- [38] G. J. Moridis, D. A. McVay, D. L. Reddell, and T. A. Blasingame, "Laplace transform finite difference (LTFD) numerical method for the simulation of compressible liquid flow in reservoirs," *SPE Advanced Technology Series*, vol. 2, no. 2, pp. 122–131, 1994.
- [39] A. D. Habte and M. Onur, "Laplace-transform finite-difference and quasistationary solution method for water-injection/falloff tests," *SPE Journal*, vol. 19, no. 3, pp. 398–409, 2014.
- [40] J. Warren and P. Root, "The behavior of naturally fractured reservoirs," *SPE Journal*, vol. 3, no. 3, pp. 245–255, 2013.
- [41] D. Bourdet, J. Ayoub, and Y. Pirard, "Use of Pressure Derivative in Well Test Interpretation," *SPE Formation Evaluation*, vol. 4, no. 02, pp. 293–302, 2013.
- [42] M. Mavor and H. Cinco-Ley, "Transient Pressure Behavior Of Naturally Fractured Reservoirs," in *Proceedings of the SPE California Regional Meeting*, Ventura, California.

